Model of transport properties of thermoelectric nanocomposite materials

A. Popescu, L. M. Woods, J. Martin, and G. S. Nolas
Department of Physics, University of South Florida, Tampa, Florida 33620, USA
(Received 17 September 2008; revised manuscript received 6 January 2009; published 5 May 2009)

We present a model describing the carrier conductivity and Seebeck coefficient of thermoelectric nanocomposite materials consisting of granular regions. The model is successfully applied to explain relevant experimental data for PbTe nanocomposites. A key factor is the grain potential boundary scattering mechanism. Other mechanisms, such as carrier-acoustic phonon, carrier-nonpolar optical phonon, and carrier-ionized impurities scattering are also included. Our calculations reveal that by changing the physical characteristics of the grains, such as potential barrier height, width, and distance between the grains, one can increase the mean energy per carrier in order to obtain an optimum power factor for improved thermoelectric performance. The model can be applied to other nanocomposites by incorporating the appropriate electronic structure parameters.

DOI: 10.1103/PhysRevB.79.205302 PACS number(s): 73.63.Bd, 72.20.Pa, 72.20.Dp

I. INTRODUCTION

The efficiency of thermoelectric (TE) devices is characterized by the thermoelectric figure of merit, defined as the dimensionless quantity $ZT=S^2\sigma T/\kappa$, where S is the Seebeck coefficient, σ is the carrier conductivity, κ is the thermal conductivity, and T is the absolute temperature. Materials with larger values of ZT warrant better thermoelectric devices, thus researchers have devoted much effort in finding ways to increase ZT. Since the transport properties that define ZT are interrelated, it is difficult to control them independently for a three-dimensional crystal. Therefore, nanostructured materials have become of great interest because they offer the opportunity of independently varying those properties.[1,2]

The reduction in the thermal conductivity in nanostructured materials has been viewed as the primary way to increase ZT. The particular mechanism is the effective scattering of phonons due to the presence of interfaces. However, recent experimental studies involving bulk thermoelectric materials with nanostructure inclusions or granular nanocomposites have suggested that the thermoelectric properties can be enhanced by increasing the power factor, $S^2\sigma$. For example, it has been demonstrated that PbTe/PbTeSe quantum dot superlattices can have a twofold increase in room temperature ZT as compared to the bulk.[3,4] Also, materials containing PbTe nanogranular formations[5,6] or Si and Ge nanoparticles[7] have also been shown to exhibit an increase in ZT.

These experimental studies indicate that the carrier scattering at the interfaces may be an important factor in the overall increase in ZT. In particular, it is speculated that for polycrystalline materials the grains appear as traps for low energy carriers, while the higher energy carriers diffuse trough the specimen.[8] In fact, the enhancement of the TE properties in nanocomposites has been attributed to the presence of carrier-interface potential barrier scattering mechanism, which is not typical for bulk materials. The grain boundaries therefore appear to filter out the lower energy carriers. Since the mean energy per carrier is increased, S increases while σ is not degraded significantly. Filtering by energy barriers has been theoretically predicted and experimentally observed in thin films and heterostructure systems.[9–11]

In this work, we propose a phenomenological model to describe the diffusion transport of carriers through a material composed of nanogranular regions. The material is viewed as containing interface potential barriers due to the grains, and the transport includes quantum transmission through and reflection from those barriers. Additional scattering mechanisms, such as carriers-acoustic phonons, carriers-nonpolar optical phonons, and carriers-ionized impurities, which are relevant for thermoelectric materials, are also taken into account. The model involves a set of physical parameters which can be measured independently or taken from the literature to calculate or make predictions for the transport characteristics for relevant thermoelectrics. The model is tested by comparing the calculated carrier conductivity and thermopower to experimental data for PbTe nanocomposites. We also use this theory to understand the importance of the grain barrier characteristics, such as height, width, and distance between them, and see to what extent they influence the thermoelectric transport.

The paper is organized as follows. The model is presented in Sec. II. In Sec. III experimental results and theoretical calculations for PbTe nanocomposite specimens are given, and σ and S are analyzed in terms of the carrier concentration and barrier characteristics. The summary and conclusions are given in Sec. IV.

II. MODEL

We consider a thermoelectric material for which the motion of the carriers is in quasiequilibrium and diffusive. Then one can describe the charge transport with the following expressions[12] for σ and S:

$$\sigma = \frac{2e^2}{3m^*}\int_0^\infty \tau(E)g(E)E\left(-\frac{\partial f(E)}{\partial E}\right)dE, \qquad (1)$$

$$S = \frac{1}{eT}\left[\frac{\int_0^\infty \tau(E)g(E)E^2\left(-\frac{\partial f(E)}{\partial E}\right)dE}{\int_0^\infty \tau(E)g(E)E\left(-\frac{\partial f(E)}{\partial E}\right)dE} - \mu\right], \quad (2)$$

where e is the electron charge, m^* - the effective mass, μ - the chemical potential for the specific material, $\tau(E)$ - the momentum relaxation time for the charge carriers, $g(E)$ - the total density of states (DOS) for the material, and $f(E)$ - the energy distribution function. The carrier conductivity and Seebeck coefficient defined in Eqs. (1) and (2) are derived from linear-response theory and they are equilibrium parameters.[12,13] $\tau(E), g(E)$, and $f(E)$ are energy-dependent functions but they also depend on other physical characteristics which are specific for each material. Below we consider each of these functions individually and explain the relevant assumptions we make here.

A. Density of states

Our model assumes that the electronic structure inside the grain formations is the same as the electronic structure of the corresponding bulk material. The grain boundary does not affect significantly the energy-band structure and it serves only as a scattering interface. This assumption is justified based on recent experiments reporting transport measurements in PbTe[6] and in SiGe.[14] The scanning electron microscope images show that the grain regions are in the range of 100 nm–1 μm and are highly crystalline.

Most thermoelectric materials are small band-gap semiconductors and the energy bands responsible for the transport are not parabolic.[12] Their Fermi surfaces are ellipsoids of revolution. It has been shown that for some small band-gap thermoelectric semiconductors the nonparabolic two band Kane model is a good description for their energy dispersion,[12]

$$\frac{\hbar^2 k_l^2}{2m_l^*} + \frac{\hbar^2 k_t^2}{2m_t^*} = E + \alpha E^2, \quad (3)$$

where $k_{l,t}$ is the carrier momentum, $m_{l,t}^*$ - the effective mass along the longitudinal and transverse directions at the valence-band minimum, respectively, and α - a nonparabolicity factor. For small band-gap semiconductors $\alpha = 1/E_g$ where E_g is the energy gap. After defining an effective mass for both directions as $m^* = \beta^{2/3}(m_l^* m_t^{*2})^{1/3}$ with β being the degeneracy of the Fermi surfaces containing more than one pocket, the total DOS can be written as

$$g(E) = \frac{\sqrt{2}}{\pi^2}\left(\frac{m^*}{\hbar^2}\right)^{3/2}\sqrt{E(1+E/E_g)}(1+2E/E_g), \quad (4)$$

$$E_g = E_g^0 + \gamma T. \quad (5)$$

Here the variation of E_g as a function of temperature is also taken into account (E_g^0 is the band gap at $T=0$ K). γ is a material specific parameter which is usually deduced from experimental measurements. For example, for PbTe $E_g^0 = 0.19$ eV and γ is measured to be $\gamma \approx 0.0004$ eV/K.[15,16]

B. Energy distribution function

We further consider the energy distribution function $f(E)$. We assume that the carrier transport is a diffusive, quasiequilibrium process. Therefore, $f(E)$ is the Fermi distribution function $f(E) = 1/(e^{(E-E_F)/k_B T}+1)$ with E_F being the Fermi level, and k_B-the Boltzmann constant.[17] Although scattering at the grain boundaries introduces deviations from thermal equilibrium, when the carriers leave the barrier the other scattering mechanisms relax the energy distribution until thermal equilibrium is reached,[18] and this is the contribution we consider here. The nonequilibrium part is not taken into account using the expressions for S and σ derived from linear-response theory (Eqs. (1) and (2)). The Fermi distribution function contains an important parameter, the Fermi level E_F, which is specific for each material. It is also related to the charge-carrier concentration, p, via the expression,[19]

$$p = \frac{4}{\sqrt{\pi}}\left(\frac{2\pi m^* k_B T}{h^2}\right)^{3/2}\int_0^\infty E^{1/2} f(E)dE, \quad (6)$$

where h is the Planck's constant. The self-consistent solution of the above equation allows one to determine the Fermi level E_F for a specific concentration p.

C. Scattering mechanisms

Finally, we consider the momentum relaxation time, $\tau(E)$, with contributions from different scattering mechanisms. Here it is assumed that each scattering mechanism can be associated with a resistivity. Then the total relaxation time is obtained according to the Mathiessen's rule,

$$\frac{1}{\tau(E)} = \sum_i \frac{1}{\tau_i(E)}, \quad (7)$$

where $\tau_i(E)$ is the relaxation time for each contributing mechanism. For thermoelectric bulk materials, the most relevant carrier scattering may be due to acoustic phonons, nonpolar optical phonons, or ionized impurities.[12] However, for TE composites containing nanostructured grains, an additional scattering mechanism from the grain interfaces has to be taken into account.

In this model, the nanocomposite specimen is assumed to have grain regions with the same average characteristics. The grain interfaces in the material are modeled as rectangular potential barriers with an average height E_b, width w, and distance between them L as shown in Fig. 1. The average values of E_b, w, and L can be inferred from experimental measurements.[18,20] The physical explanation of the formation of each boundary is that each grain boundary creates an interface density of traps,[21,22] which is assumed to be electrically neutral until carriers are trapped, thus forming a potential barrier with height E_b.

The diffusion transport process we are describing concerns motion of the carriers with energy E impeding on the barriers. Let the transmission probability for the charge car-

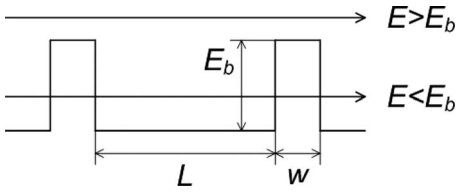

FIG. 1. Schematic of a grain region limited by rectangular potential barriers. The height of the barrier is E_b, the width -w, and the distance between the barriers -L. The carrier energy is E.

riers through a single barrier be T(E). The path length of the carriers passed through the first barrier and scattered by the second one is given by $T(E)(1\text{-}T(E))L$. The carrier path length after passing through the second and scattering from the third barrier is $T(E)^2(1\text{-}T(E))2L$. Thus the mean-free path after scattering from N barriers becomes[23,24]

$$\lambda = \sum_{n=1}^{N\to\infty} T(E)^n(1\text{-}T(E))nL = \frac{T(E)L}{1\text{-}T(E)}. \tag{8}$$

Assuming that there is practically an infinite number of barriers, the summation over the barriers can be performed, as shown in Eq. (8). Then the relaxation time due to the barrier scattering is given by

$$\tau_b(E) = \frac{\lambda}{v}, \tag{9}$$

where $v = \sqrt{\frac{2E}{m^*}}$ is the average velocity of the charge carriers.

Furthermore, the expression for the transmission probability through a single barrier can easily be obtained following standard quantum-mechanical considerations by taking that the incident carriers upon the barrier are plane-wave-like.[25] For the situations when the carrier energy is smaller ($E < E_b$) or larger ($E > E_b$) than the barrier height, one finds

$$\tau_b(E) = \begin{cases} L\sqrt{\frac{m^*}{2E}}\left[1 + \frac{4\frac{E}{E_b}\left(1-\frac{E}{E_b}\right)}{\sinh^2\left[\sqrt{\frac{2m^*E_bw^2}{\hbar^2}\left(1-\frac{E}{E_b}\right)}\right]}\right], E < E_b \\ L\sqrt{\frac{m^*}{2E}}\left[1 + \frac{4\frac{E}{E_b}\left(\frac{E}{E_b}-1\right)}{\sin^2\left[\sqrt{\frac{2m^*E_bw^2}{\hbar^2}\left(\frac{E}{E_b}-1\right)}\right]}\right], E > E_b \end{cases}. \tag{10}$$

The relaxation times due to the other mechanisms can be expressed as

$$\tau(E) = aE^s, \tag{11}$$

where $s = -\frac{1}{2}, \frac{1}{2}, \frac{3}{2}$ for carrier scattering by acoustic phonons, nonpolar optical phonons, and ionized impurities, respectively. The parameter a is temperature dependent and we use the expressions,[26]

$$a_{\text{a-ph}} = \frac{h^4}{8\pi^3}\frac{\rho v_L^2}{k_BT}\frac{1}{(2m^*)^{3/2}D^2},$$

$$a_{\text{o-ph}} = \frac{h^2}{2^{1/2}m^{*1/2}e^2k_BT(\varepsilon_\infty^{-1} - \varepsilon_0^{-1})},$$

$$a_{\text{imp}} = \left[\frac{Z^2e^4N_i}{16\pi(2m^*)^{1/2}\varepsilon^2}\ln\left[1 + \left(\frac{2E}{E_m}\right)^2\right]\right]^{-1}, \tag{12}$$

where $a_{\text{a-ph}}$, $a_{\text{o-ph}}$, and a_{imp} are the constants for the acoustic phonons, nonpolar optical phonons, and ionized impurities, respectively. Also, ρ is the mass density, v_L-the longitudinal velocity of sound, D-the deformation-potential constant, ε_∞-the high-frequency dielectric constant, ε_0-the static dielectric constant, and ε-the dielectric constant of the medium. In addition, $E_m = \frac{Ze^2}{4\pi\varepsilon r_m}$ is the potential energy at a distance r_m from an ionized impurity with r_m approximately half the mean distance between two adjacent impurities, and N_i is their concentration. These quantities can be taken from the available data in the literature or estimated experimentally for a particular specimen. The value for D is usually adjusted when phenomenological models are used to explain experimental measurements. However, D can also be estimated independently by measuring the changes in E_g of a specific material as a function of pressure and temperature.[26]

III. RESULTS

The model described in Sec. II provides all the necessary tools to calculate and explain the experimental data for σ and S for small band-gap semiconducting TE materials containing granular interfaces. The applicability of the model lies within the assumption that the carrier transport is quasiequilibrium and diffusive, thus the use of Eqs. (1) and (2) and the Fermi distribution function is justified. The relaxation-time approximation, which describes each scattering mechanism independently of the others, is also taken to be valid. The

model also contains a set of physical parameters and constants which can be taken from available experimental data for a specific material or they can be measured for a specific specimen. These are the effective mass m^*, the band gap E_g, the dielectric constants ε_0 and ε_∞, the mass density ρ, the longitudinal velocity of sound v_L and the deformation-potential constant D. Furthermore, we have considered that the energy-band structure of the granular regions is the same as their bulk counterparts and the nonparabolic two-band Kane model is an adequate description for it. The former assumption is motivated by experimental results for the thermoelectric transport for PbTe and SiGe nanocomposites reported recently,[6,14] which show that the size of the granular regions is 100 nm-1 μm and they are highly crystalline. The latter assumption is based on previous studies which have shown that for some small band-gap semiconductors with good TE characteristics, such as the IV-VI compounds,[27] the two-band Kane model with nonparabolicity taken into account through the band gap ($\alpha=1/E_g$) gives adequate description for the TE transport. Thus our model can be used for a small band-gap semiconducting TE nanocomposite with a diffusive transport through the granular regions with bulklike two-band energy structure simply by specifying the physical parameters listed above and executing the calculations for σ and S [Eqs. (1) and (2)].

Here we demonstrate how effectively this model can be used to describe experimental data for PbTe nanocomposite material. The model is tested by comparing to low-temperature transport measurements for Ag-doped PbTe nanocomposites, prepared in the following method. Lead telluride nanocrystals were synthesized employing an aqueous solution-phase reaction by mixing a Te-KOH aqueous solution and lead acetate trihydrate $[Pb(CH_3COO)_2\cdot 3H_2O]$ solution at low temperature and standard atmosphere.[6] The Ag-doped PbTe nanocrystals were prepared by dissolving a Ag compound in the $[Pb(CH_3COO)_2\cdot 3H_2O]$ solution to achieve the desired carrier concentration. This procedure reproducibly synthesizes 100–150 nm spherical PbTe nanocrystals, confirmed by TEM, with a high yield of over 2 g per batch. These nanocrystals were subjected to Spark Plasma Sintering to achieve ~95% bulk theoretical density, resulting in a dimensional nanocomposite structure,[6] as observed in scanning electron microscope images of both fracture and polished surfaces. The presence of ionized impurities in the samples is not significant.

Four-probe resistivity and steady-state gradient sweep Seebeck coefficient were measured from 12 to 300 K in a custom radiation-shielded vacuum probe with maximum uncertainties of 4% and 6%, respectively, at 300 K.[28] Room-temperature four-probe Hall measurements were conducted at multiple positive and negative magnetic fields to eliminate voltage probe misalignment effects and thermal instabilities with a 10% uncertainty.

The experimental results for the carrier conductivity for two Ag-doped specimens with carrier concentration $p=6.1\times10^{18}$ cm^{-3} and $p=5.9\times10^{18}$ cm^{-3} at 300 K are shown in Fig. 2(a). In Fig. 2(b), the experimental data for S is also given. In addition, σ and S are calculated using Eqs. (1) and (2), and shown in Figs. 2(a) and 2(b), respectively. Since the synthesized and measured samples did not contain significant

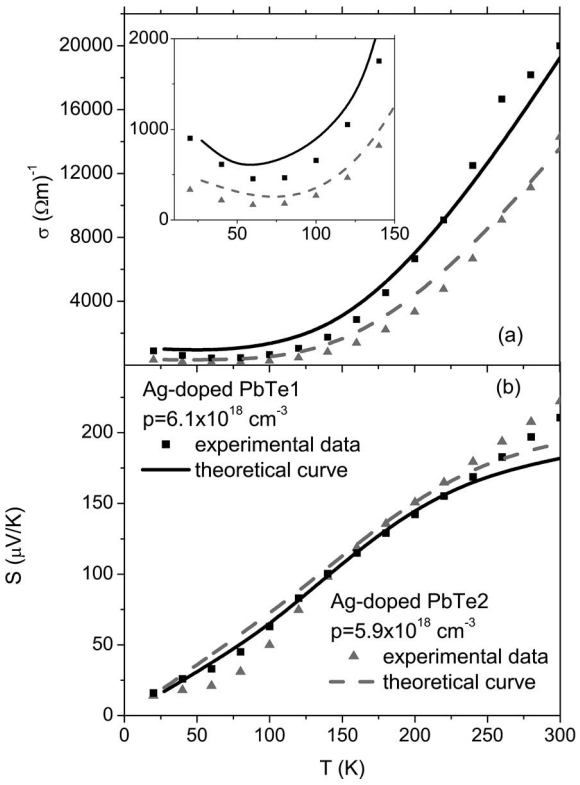

FIG. 2. Calculated and experimentally measured (a) electrical conductivity σ, and (b) Seebeck coefficient S as a function of the absolute temperature T for two values of the carrier concentrations.

concentration of ionized impurities, the carriers-impurity scattering mechanism is not taken into account in our calculations. We used the following barrier parameters estimated from the reported experimental data: $E_b=60$ meV, $w=50$ nm, and $L=300$ nm.[29] The other parameters used are $m^*=0.16m_0$, where m_0 is the electron mass,[5] $\rho=8160$ kg/m^3, $v_L=1730$ m/s,[12] and $\varepsilon_\infty^{-1}-\varepsilon_0^{-1}=0.0072\times E_g$. The value for D is varied in the range 5–15 eV, as it is usually done when phenomenological models are used to compare with experimental data.[12] As shown in Fig. 2, there is excellent agreement between the experimental results for the PbTe specimens and the model calculations in all temperature regions.

The model is further used to understand the importance of the different material characteristics that affect the transport properties. We investigate the role of carrier concentration p on σ and S. Here we also consider the case when the TE granular nanocomposites contain ionized impurities. Thus the carrier-impurity scattering mechanism neglected earlier is explicitly included now. The material dependant constants (effective mass, band gap, dielectric constants, mass density, longitudinal velocity of sound, deformation-potential constant) are taken to be the same as the ones for PbTe. If one studies a granular nanocomposites made of a different small band gap semiconducting TE material, then the appropriate material dependent constants need to be taken. The potential boundary characteristics are chosen to be $E_b=0.1$ eV, $w=50$ nm, and $L=300$ nm. The calculated results are presented in Figs. 3(a) and 3(b). The figures show that σ and S

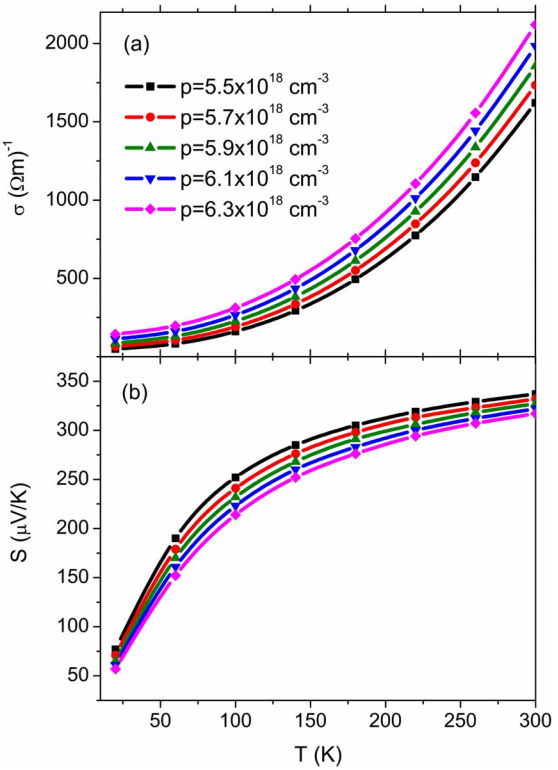

FIG. 3. (Color online) (a) Electrical conductivity, σ, and (b) Seebeck coefficient, S, as a function of the absolute temperature T for different values of the carrier concentrations. The impurity concentration is $N_i=15\%p$.

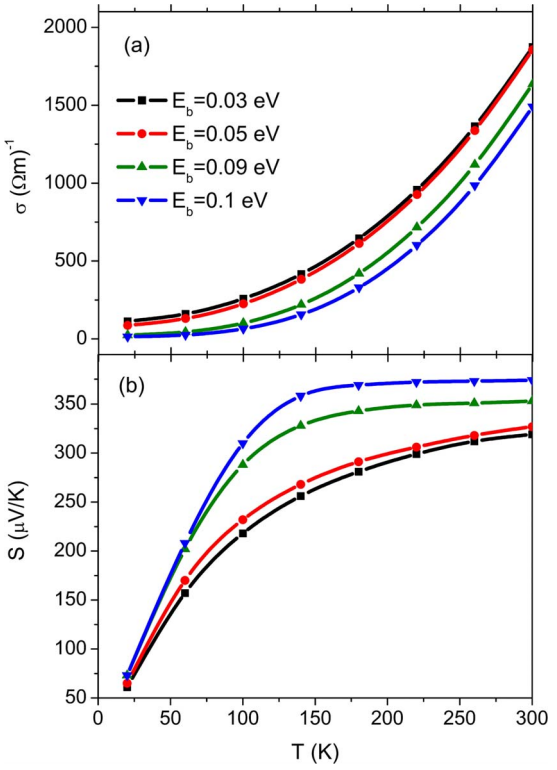

FIG. 4. (Color online) (a) Electrical conductivity, σ, and (b) Seebeck coefficient, S, as a function of the absolute temperature T for different values of the potential barrier height.

increase as a function of temperature. The functional dependence of σ vs T and S vs T is similar for all studied carrier concentrations. However, σ is larger for larger p due to the increased number of carriers, while S is larger for smaller p due to the higher mean energy per carrier.

Using this theory, we also investigate how other parameters, related to the grain-boundary specifications, affect the transport characteristics. From Eqs. (1) and (2) one can calculate σ and S as a function of temperature for various barrier heights, barrier widths, and distances between the barriers. In Fig. 4, we show the calculated results for σ and S as a function of temperature for several values of the barrier height, while fixing the other barrier parameters to $w=50$ nm and $L=300$ nm. The impurity scattering mechanism is also included and $N_i=15\%p$. The figure reveals that as E_b increases, the conductivity decreases while the opposite trend is found in S. We explain this by noting that higher barriers will scatter carriers with larger energy E [Eq. (10)], therefore less carriers will contribute to the electrical current. The same filtering process will contribute to the increase in the energy per carrier leading to an increased Seebeck coefficient for barriers with larger height.

We can achieve the same physical behavior by changing w or L. For example, increasing w results in a decrease in σ and an increase in S due to the smaller quantum-mechanical transmission probability of the carriers through the barrier [Eq. (10)]. Furthermore, decreasing L results in decreasing σ and increasing S due to more frequent carrier scattering from the barriers. From Eqs. (1) and (2) the dependence of σ and S for various w and L show similar behavior as that described above.

Experimentally one may be able to change different parameters characterizing the potential grain barriers in order to manipulate the carrier transport characteristics as a function of temperature. For thermoelectric applications, however, one is interested in increasing the power factor $S^2\sigma$. Thus the optimal E_b, w, and/or L are needed to achieve such σ and S in order to obtain the highest performing TE materials. Our model can be applied to investigate the role of the barrier parameters and determine a range of their values for optimal TE transport. Thus calculating $S^2\sigma$ as a function of E_b, w, or L is very advantageous compared to experimentally synthesizing different samples and measuring each one of them.

We calculated $S^2\sigma$ using Eqs. (1) and (2) in order to show how $S^2\sigma$ varies as a function of E_b, w, and L at a specific temperature. All scattering mechanisms are included. Our results for $T=300$ K are presented in Fig. 5. Similar functional dependences are found for other temperatures. Figure 5(a) shows that the power factor quickly increases until $E_b \approx 0.04$ eV. After that, $S^2\sigma$ increases at a much slower rate until $E_b \approx 0.1$ eV. For $E_b > 0.1$ eV, the power factor decreases. Figures 5(b) and 5(c) show that the power factor has the most pronounced changes around $w=55$ nm and $L=250$ nm.

The fact that the power factor exhibits such behavior as well as the results for σ and S shown in Figs. 3 and 4, reveals that carrier charge and energy transport may or may not be affected in a beneficial way by varying the nanocomposite grain characteristics. If more charge carriers (lower E_b), less

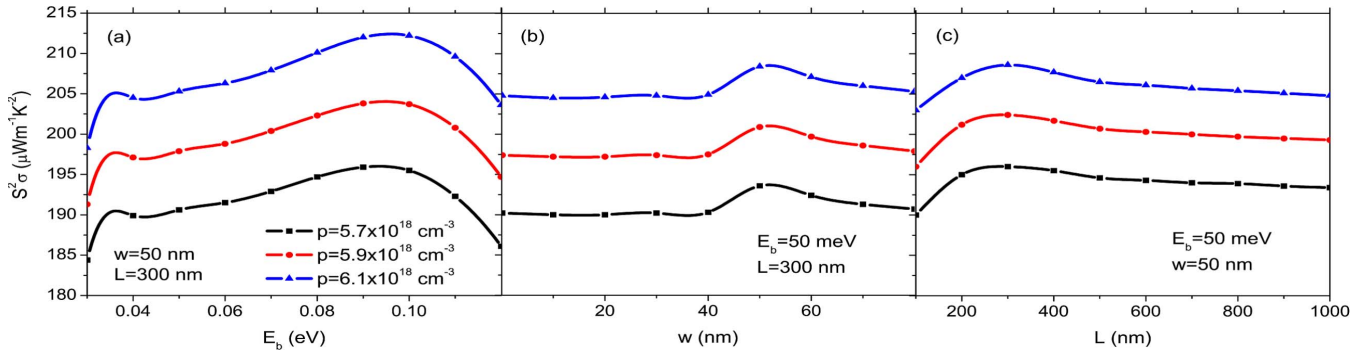

FIG. 5. (Color online) Power factor as a function of (a) barrier height, (b) barrier width, and (c) grain size, at $T=300$ K, for three values of the carriers concentration.

frequent scattering (longer L), and larger transmission through the barrier (smaller w) are allowed, the electrical conductivity increases. In contrast, when the mean energy per carrier is increased by taking higher barriers (larger E_b), more frequent scattering (smaller L), and smaller transmission (larger w), the Seebeck coefficient increases. The reason for these two competing effects is unambiguously related to the expressions for $\tau_i(E)$ and the DOS—Eqs. (4), (7), and (10). Therefore, the key issue is to have TE nanocomposites with such grain characteristics that can balance the interplay between increasing S and at the same time not decreasing σ too much to obtain an overall increase in the power factor. This theoretical approach shows explicitly how E_b, w, and L can be changed in order to achieve the best TE performance for a given polycrystalline thermoelectric material.

IV. CONCLUSIONS

A model for describing the diffusive transport properties in granular nanocomposite materials was proposed and successfully applied to explain relevant experimental data. The interfaces of the nanoscaled granular regions are modeled as rectangular barriers. The transport through the material includes carrier quantum-mechanical transmission and scattering from the barriers, carrier-phonon and carrier-ionized impurities scattering within the grains. The theoretically calculated σ and S can reproduce the experimental observations obtained for Ag-doped PbTe and undoped PbTe nanocomposite specimens. We have shown that the interplay between the different scattering mechanisms, as well as the carrier concentration and the physical parameters for the barriers, are important in finding an optimal regime for the TE performance of a given material. Specifically, our model reveals that by manipulating the barrier size and height, the mean energy per carrier may be increased leading to an increase in S without substantial degradation of σ. Furthermore, the model can be adapted for other material systems composed of highly crystalline grains without or with appropriate doping. Particular examples could be InSb, $CoSb_3$, or CdSe composites. For all three materials, the relevant assumptions made here in terms of a two-band energy-band structure model, relaxation-time approximation, and important scattering mechanisms are valid. By incorporating their appropriate physical parameters, such as band gaps, effective masses, dielectric constants, and deformation-potential constants, the model may be used to predict the thermoelectric performance of these particular granular composites and thus serve as a guide for future experimental efforts. Furthermore, the model can be extended for composites which cannot be described by the two-band Kane model by modifying the description of the DOS and including all relevant energy bands contributing to the thermal transport.

ACKNOWLEDGMENTS

The authors acknowledge support by the U.S. Army Medical Research and Material Command under Award No. W81XWH-07-1-0708. Opinions, interpretations, conclusions, and recommendations are those of the authors and are not necessarily endorsed by the U.S. Army.

[1] G. S. Nolas, J. Sharp, and H. J. Goldsmid, *Thermoelectrics: Basic Principles and New Materials Developments* (Springer, New York, 2001).
[2] G. Chen, M. S. Dresselhaus, G. Dresselhaus, J. P. Fleurial, and T. Caillat, Int. Mater. Rev. **48**, 45 (2003).
[3] T. C. Harman, P. J. Taylor, M. P. Walsh, and B. E. LaForge, Science **297**, 2229 (2002).
[4] T. C. Harman, M. P. Walsh, B. E. LaForge, and G. W. Turner, J. Electron. Mater. **34**, L19 (2005).
[5] J. P. Heremans, C. M. Thrush, and D. T. Morelli, Phys. Rev. B **70**, 115334 (2004).
[6] J. Martin, G. S. Nolas, W. Zhang, and L. Chen, Appl. Phys. Lett. **90**, 222112 (2007).
[7] M. S. Dresselhaus, G. Chen, M. Y. Tang, R. G. Yang, H. Lee, D. Z. Wang, Z. F. Ren, J. P. Fleurial, and P. Gogna, Mater. Res. Soc. Symp. Proc. **886**, 3 (2006).
[8] Y. I. Ravich, *CRC Handbook of Thermoelectrics* (CRC, New York, 1995).

[9] D. Vashaee and A. Shakouri, Phys. Rev. Lett. **92**, 106103 (2004).
[10] D. Vashaee and A. Shakouri, J. Appl. Phys. **95**, 1233 (2004).
[11] G. D. Mahan and L. M. Woods, Phys. Rev. Lett. **80**, 4016 (1998).
[12] D. M. Rowe and C. M. Bhandari, *Modern Thermoelectrics* (Holt Saunders, London, 1983).
[13] Yu. I. Ravich, B. A. Efimova, and I. A. Smirnov, *Semiconducting Lead Chalcogenides* (Plenum, New York, 1970).
[14] G. Joshi, H. Lee, Y. Lan, X. Wang, G. Zhu, D. Wang, R. W. Gould, D. C. Cuff, M. Y. Tang, M. S. Dresselhaus, G. Chen, and Z. Ren, Nano Lett. **8**, 4670 (2008).
[15] M. L. Cohen and J. R. Chelikowsky, *Electronic Structure and Optical Properties of Semiconductors*, Springer Series in Solid State Sciences, 2nd ed., edited by M. Cardona (Springer-Verlag, Berlin, 1989) Vol. 75.
[16] R. Dalven, in *Solid State Physics*, edited by H. Ehrenreich, F. Seitz, and D. Turnbull (Academic, New York, 1973), Vol. 28, p. 179.
[17] G. D. Mahan, *Many-Particle Physics*, 3rd ed. (Plenum, New York, 2000).
[18] K. Kishimoto and T. Koyanagi, J. Appl. Phys. **92**, 2544 (2002).
[19] A. K. Sreedhar and S. C. Gupta, Phys. Rev. B **5**, 3160 (1972).
[20] K. Kishimoto, K. Yamamoto, and T. Koyanagi, Jpn. J. Appl. Phys., Part 1 **42**, 501 (2003).
[21] R. E. Jones and S. P. Wesolovski, J. Appl. Phys. **56**, 1701 (1984).
[22] C. H. Seager, J. Appl. Phys. **52**, 3960 (1981).
[23] Sh. B. A. Atakulov and A. N. Shamsiddinov, Solid State Commun. **56**, 215 (1985).
[24] Y. Nishio and T. Hirano, Proceedings ICT98, 17th International Conference in Thermoelectrics, Nagoya, Japan, 1998, p. 111–114.
[25] N. Zettili, *Quantum Mechanics: Concepts and Applications* (Wiley, Chichester, 2001).
[26] C. M. Bhandari and D. M. Rowe, *Thermal Conduction in Semiconductors* (Wiley, New York, 1988).
[27] H. Kawamura, *Narrow Gap Semiconductors; Physics and Applications* (Springer, Berlin, 1980).
[28] J. Martin, G. S. Nolas, H. Wang, and J. Yang, J. Appl. Phys. **102**, 103719 (2007).
[29] J. Martin, L. Wang, L. Chen, and G. S. Nolas, Phys. Rev. B **79**, 115311 (2009).